Pergamon

Scripta Materialia, Vol. 39, Nos. 4/5, pp. 457–464, 1998
Elsevier Science Ltd
Copyright © 1998 Acta Metallurgica Inc.
Printed in the USA. All rights reserved.
1359-6462/98 $19.00 + .00

PII S1359-6462(98)00222-X

DECOMPOSITION OF a<111> AND a<101> DISLOCATIONS IN HARD-ORIENTED NiAl SINGLE CRYSTALS

R. Srinivasan, M.F. Savage, M.S. Daw*, R.D. Noebe# and M.J. Mills
Department of Materials Science and Engineering, The Ohio State University, Columbus, OH 43210
*Department of Physics and Astronomy, Clemson University, Clemson, SC 29634-1911
#NASA Lewis Research Center, Cleveland, OH 44135

(Received in final form May 15, 1998)

Introduction

The B2 intermetallic compound NiAl and its alloys have been subjects of extensive study for potential use as high temperature structural materials, particularly in the aerospace industry. The factors that make them attractive candidates are their low density (5.85 g/cm^3), excellent oxidation and corrosion resistance and high melting points. But they suffer from lack of ductility at low temperatures and poor strength at higher temperatures. Due to recent advances in both areas [1,2], active interest in NiAl alloys continues. In particular, in spite of extensive study, the precise dislocation processes operative under a variety of conditions remain uncertain.

There are still several issues regarding deformation behavior in NiAl and other B2 alloys (e.g. FeAl) that merit further research. Study of the deformation behavior in NiAl should provide further insight into some of the outstanding issues in B2 alloys: chiefly, the nature of slip transition and the effect of various parameters such as temperature, strain rate and stoichiometry on the deformation behavior. The preferred slip system in NiAl involves a<100> slip. But on stressing along the cube axes, also known as the "hard" orientation, single crystals of NiAl deform at much higher stresses through the motion of a<111> dislocations at lower temperatures. Non-a<111> slip dominates at higher temperatures, with an associated increase in ductility and dramatic decrease in strength [3,4]. There is also some confusion regarding the mode of deformation beyond the slip transition temperature. The exact process of this slip transition needs to be addressed in its entirety to completely understand the mechanical response of NiAl.

Experimental

Single crystals of Ni-50Al and Ni-44Al were grown by a Bridgmann technique. They were tested in compression in the "hard" orientation over a range of temperature and strain levels (at a strain rate of 10^{-4}/s), encompassing the slip transition temperature (in order to understand the mechanism of slip transition). Thin foils for TEM investigation were prepared by cutting slices on a low speed diamond saw, then polishing in a twin-jet electropolisher at a current of 25–30 mA and a voltage of 6–8 V. Transmission Electron Microscopy (TEM) investigations were performed on a Philips CM 200 (LaB_6 cathode) operating at 200 kV and a Philips EM 400 operating at 120 kV.

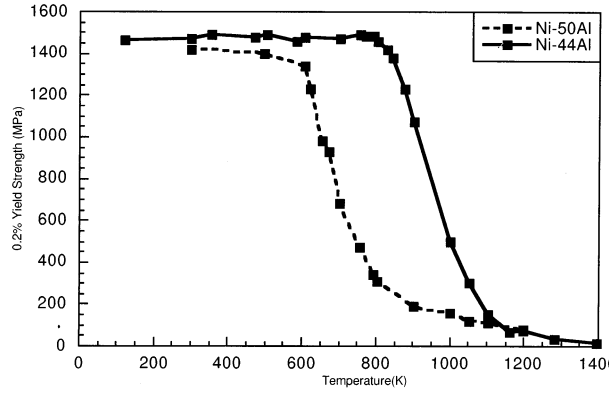

Figure 1. Yield strength vs. temperature for hard-oriented Ni-44Al and Ni-50Al.

Results and Discussion

Mechanism of Slip Transition

Figure 1 shows the yield strength as a function of temperature for hard-oriented Ni-44Al and Ni-50Al. The slip transition is associated with the sharp drop in yield strength (and also corresponds to the onset of significant tensile ductility at the same temperature [4]). The slip transition for Ni-44Al occurs at a dramatically higher temperature (800 K) than for binary NiAl (600 K).

To understand the mechanism of this slip transition, the deformation microstructure in Ni-44Al was studied from 750 K through 900 K, at temperature intervals of 25 K. Figure 2 shows the typical microstructure at 750 K, at a strain level of 0.7%. The dominant mode of slip is a<111>{110}. The arrows in Figure 2 indicate the cusp-like features in the dislocation segments, which are possible sites of local decomposition of the a<111> dislocations. Decomposition can occur (by glide) according to:

$$a\langle 111\rangle \longrightarrow a\langle 101\rangle + a\langle 010\rangle \quad (1)$$

The above reaction is energetically favorable within about 30° of the edge orientation [5], which is the prominent orientation in Figure 2. The line energy for a<111> dislocations is minimum along screw orientation, and increases monotonically to maximum for edge character [6].

In principle, this decomposition reaction should be favored for all temperatures. But a<111> dislocations continue to control deformation up to approximately 800 K (in Ni-44Al). Figure 3 shows the dislocation microstructure in Ni-44Al after deformation at 800 K. Note that the a<101> and a<010> dislocations that dominate the microstructure add up to the a<111> dislocations on the same glide plane, providing further proof for glide decomposition. Several outstanding questions arise on observing these deformation microstructures: (1) Why is complete decomposition of a<111> dislocations temperature dependent, (2) Why do a<101> dislocations contribute to deformation only beyond the slip transition temperature, and (3) What is the role of stoichiometry in the a<111> decomposition/slip transition process? An elementary model is presented below explaining the process of a<111> decomposition leading to slip transition, based on microstructural observations in Ni-44Al.

Two noteworthy facts emerge from Figure 1: (a) below the "knee" in the yield strength vs. temperature curve (i.e. the temperature of the slip transition), the behavior is nearly athermal, and (b) above the "knee," the yield strength decreases sharply with temperature. Let us assume that deformation by a<101> dislocations is controlled by their mobility, which in turn is strongly dependent on temperature (the possible source of which is discussed below). The athermal behavior of the yield

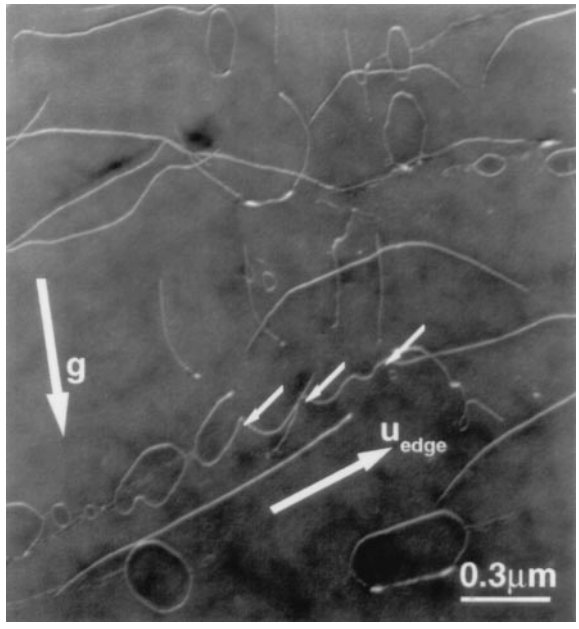

Figure 2. g(110) weak-beam g-3g micrograph near the [001] zone in a Ni-44Al sample strained 0.7% at 750K, showing cusp-like features (indicated by arrows) in near-edge a[111] segments. The cusps are possible local decomposition sites. The glide plane for the a[111] segments is $(0\bar{1}1)$, and the line direction u_{edge} for the pure edge segments is $[\bar{2}11]$.

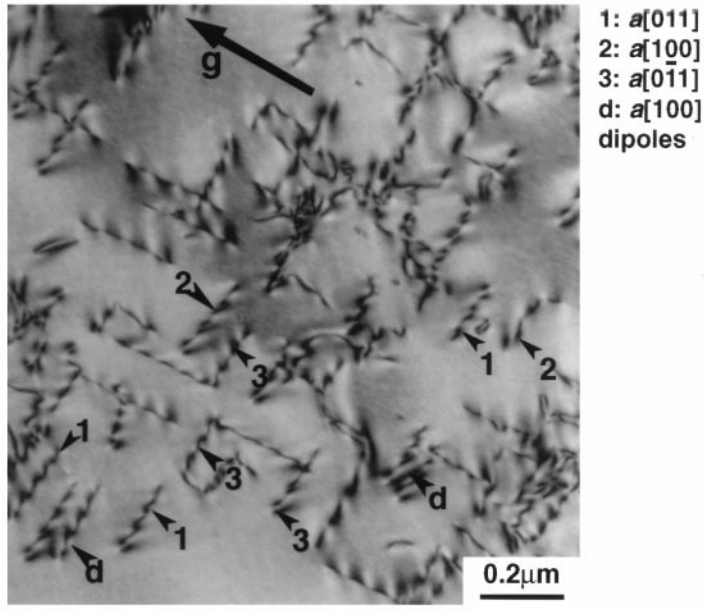

Figure 3. g(110) bright field micrograph showing the dislocation structure in Ni-44Al strained 1.7% at 800 K. The beam direction is close to [001].

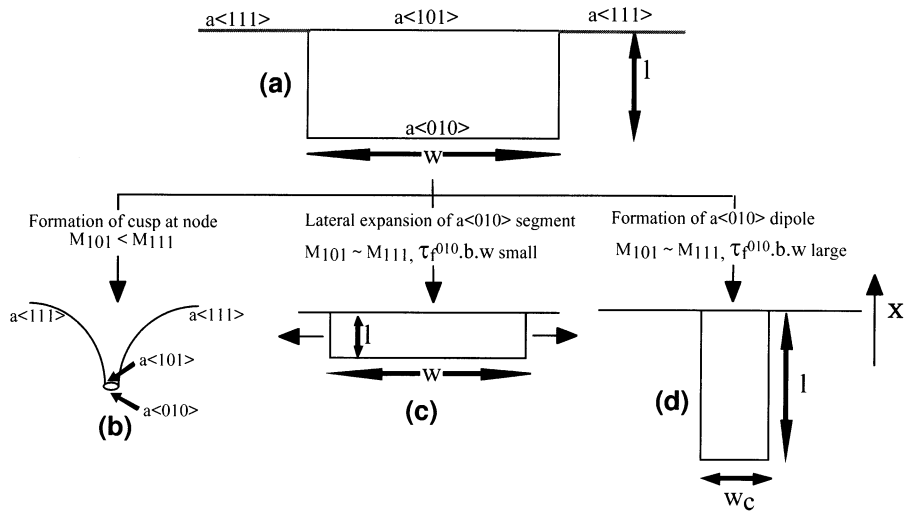

Figure 4. Schematic diagram showing the possible scenarios during decomposition of an a<111> dislocation: (a) Schematic magnified view of decomposed node, (b) Formation of a cusp at the decomposed node, if mobility of a<111> dislocation is greater than for a<101> dislocation, (c) Lateral expansion of node till w reaches w_c, and (d) Extension of the node after w has reached w_c.

strength below the "knee" suggests no effect of thermal activation on mobility of a<111> dislocations. Below the slip transition temperature, the mobility of a<111> dislocations is therefore much higher than that for a<101> dislocations; consequently, a<111> dislocations can dominate the deformation microstructure. Assuming that a decomposition event can occur near the edge orientation, a local decomposition node would serve as a pinning point below the "knee," since the a<101> and a<010> segments created at the node would be immobile. The remainder of the undecomposed a<111> segment would be able to glide, eventually creating a cusp at the local decomposition node, as indicated by the arrows in Figure 2. Figure 4a shows a schematic view of the decomposed node. Figure 4b shows a schematic view of the formation of cusps due to the decomposition node.

At higher temperatures, the mobilities of the a<111> and a<101> segments can become comparable. The a<111> dislocation and the a<101> segment can then glide at the applied stress level. But the a<010> segment will be relatively immobile, since it has no macroscopic stress on it. In such a case, the immobile a<010> segment can be dragged along with the moving a<111>-a<101> combination as in Figure 4c. The lateral expansion of the a<010> loop could then lead to complete decomposition of the a<111> dislocation line. Alternatively, an a<010> dipole can be dragged out, assuming a relatively high friction stress on the a<010> segment along the decomposition line direction, as in Figure 4d.

An approximate elasticity treatment will now be described which provides insight into the extent to which these possible scenarios will occur. In this treatment, we consider a decomposition node of width *w* and length *l* of the dipole segment, as indicated in Figure 4a. The line energies calculated using anisotropic elasticity theory [7] for the various dislocations along their direction of observation are listed in Table 1.

We have calculated the following expressions for the interaction forces per unit length for decomposition (F_{decomp}) and dipole attraction (F_{dip}) using anisotropic elasticity theory and assuming the <111> line direction which is predominantly observed in Figure 3 (for which the <101> dislocation is of 35° character and the <010> is of 55° character):

TABLE 1
Line Energies of Various Dislocations Along Observed Orientations. The Data is Obtained from Glatzel et al. [7].

b	u	Energy (10^{-9} J/m)
[111]	$[1\bar{1}1]$	20.5
[101]	$[1\bar{1}1]$	9.3
[010]	$[1\bar{1}1]$	5.9

$$F_{decomp} = 0.4496 \times 10^{-9}/l \text{ (in N/m)} \tag{2a}$$

$$F_{dip} = -1.006 \times 10^{-9}/w \text{ (in N/m)} \tag{2b}$$

The forces are calculated for infinitely long dislocations, and thus ignore the finite length of the actual segments, as well as interactions between non-parallel segments.

The virtual work expended in the process of moving the a<010> half loop a distance dx along with the gliding <101> segment (as in Figure 4c) is given by:

$$-\frac{dW}{dx} = [(\tau - \tau_f^{101}) \cdot b^{101} + F_{decomp}] \cdot w + [\tau_f^{010} \cdot b^{010} - F_{decomp}] \cdot w \tag{3}$$

where τ is the applied shear stress, τ_f^{101} is the friction stress on the a<101> segment, and τ_f^{010} is the friction stress on the a<010> segment. The work done in extending the a<010> dipole behind the gliding a<101> segment by a distance dx (as in Figure 4d) is given by:

$$-\frac{dW}{dx} = [(\tau - \tau_f^{101}) \cdot b^{101} + F_{decomp}] \cdot w + 2E^{010} \tag{4}$$

where E^{010} is the energy per unit length of the a<010> segment along the dipole direction. A third consideration is the change in energy upon an incremental, lateral expansion dw of the a<010> dipole, which will be driven by the reduction in self energies of the various line segments:

$$-\frac{dW}{dw} = -E^{111} + E^{101} + E^{010} + 2\tau_f^{010} \cdot b^{010} \cdot l + F_{dip} \cdot l \tag{5}$$

where E^{111} and E^{101} are the energy per unit length for the a<111> and the a<101> segments, respectively. F_{dip} is the force of attraction between the dipole segments. Note here that dW/dx is zero.

$$\text{At equilibrium, } l_c = \frac{E^{111} - E^{101} - E^{010}}{2\tau_f^{010} \cdot b^{010} + F_{dip}} \tag{6}$$

where l_c is the critical length of the dipoles. Expansion of the dipole will occur for $l < l_c$, and stop when $l = l_c$. At equilibrium between a moving a<010> dislocation and dipole extension,

$$w_c = \frac{2E^{010}}{\tau_f \cdot b^{010} - F_{decomp}} \tag{7}$$

Initially, a small decomposition node will expand laterally (increase *w*) until the node width reaches w_c. Thereafter, extension (increasing *l*) can occur until l reaches l_c, while the width remains fixed at w_c. As the dipole length increases beyond l_c, the width will start decreasing because the dipole attraction force is now more powerful than the decomposition force for expansion. This simple analysis therefore suggests that complete decomposition of the a<111> line cannot initiate at a single decomposition

node, provided the a<010> friction stress has a finite value. Instead, for complete decomposition to occur, multiple decomposition nodes would have to form, separated by a distance less than w_c (neglecting the attractive forces between a<010> segments of adjoining dipoles). Note that in such a case, the dipoles can annihilate before reaching the critical length l_c. This would result in separate a<101> and a<010> segments, which are the final products of decomposition of the parent a<111> dislocations as observed in Figure 3.

Assuming a friction stress of 200 MPa for the a<010> segment along the observed line direction for decomposition, a critical decomposition node width (w_c) of 0.225μm is obtained for extension of the a<010> dipole. Figure 3 shows a number of a<010> dipoles that lend support to the above model. The measured dipole separation length is between 0.04–0.08μm, with an average separation around 0.05μm. This is much smaller than that predicted with these calculations, but it should be noted that the above calculations are only approximate, particularly with respect to the interaction forces. A more complete model of this process is presently being developed.

Activity Beyond the Slip Transition Temperature

At T > 800 K in Ni-44Al, a<101> mobility apparently exceeds the a<111> mobility, and thus a<101> dislocations become the dominant species. This assumption is evidenced by the large density of a<101> dislocations seen in Figure 3, and that their density relative to a<010> dislocations is observed to increase at larger strains. Therefore, multiplication and subsequent glide of a<101> dislocations appears to dominate in this regime just above the "knee." The deformation characteristics of interest in this regime include flow softening and strong temperature and strain rate dependence. A model for a<101> dislocation motion has been developed which accounts for these characteristics [8].

This model is based on the observed [9] fact that a<101> dislocations themselves tend to decompose as given below:

$$a\langle 101\rangle \longrightarrow a\langle 100\rangle + a\langle 001\rangle \tag{8}$$

Upon consideration of line energies, elastic interactions and core effects, through a combination of continuum elasticity theory and Embedded Atom Method (EAM) calculations, the above reaction is found to be energetically favorable only along edge character [8]. For all other line directions, this reaction is unfavorable as strong attractive forces exist between the product a<010> dislocations. No such restoring forces exist for the edge orientation, so that the a<010> dislocations can climb apart from each other. In this event, overall glide motion of the a<101> dislocation requires the lateral glide of non-edge components of the a<101> dislocation. An illustration of such a model is shown in Figure 5a. This lateral motion of the kinks would be resisted by the climb-decomposed edge segments, requiring that they zip back together. Note that these climb processes could be mediated by pipe diffusion since the a [100] is linked to the a [001], and can act as a vacancy source and sink respectively, during decomposition. Since glide motion is restrained by these climb-decomposed segments, a dislocation velocity law based on this model will naturally exhibit a large temperature dependence, as is observed experimentally. A final attractive qualitative feature of this a<101> diffusion mediated glide model is that the decomposition products may continue to separate, provided that they are not zipped back together by a gliding non-edge segment, as shown in Figure 5b. Since decomposition by climb should be more rapid at higher temperatures, this scenario can explain why the a<101> dislocations are observed only within a temperature window just above the "knee," and that independent climb of the a<010> dislocations takes over at higher temperatures.

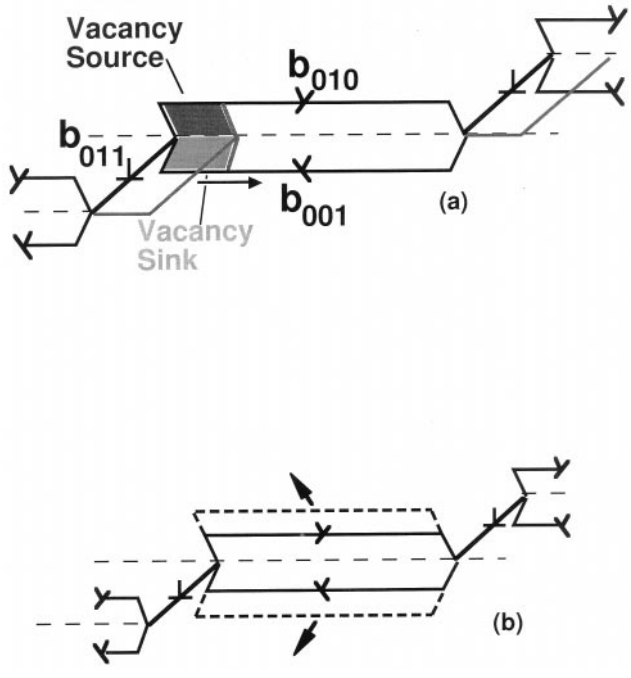

Figure 5. (a) Lateral glide of an a[011] segment by formation of a macrokink. Arrow indicates the direction of motion of the segment, and (b) Climb of individual a<010> components leading to decomposition of a<011> dislocation.

Effect of Stoichiometry

An outstanding feature of Figure 1 which remains unresolved is the dramatic shift in the temperature of the "knee" with deviation from stoichiometry. We have argued above that the decomposition of the a<111> dislocation is controlled by its mobility relative to that for the a<101> segment and, therefore, if the mobility of the a<101> were higher for the stoichiometric composition, then decomposition might occur at a lower temperature. In contradiction with this possibility is the fact that few a<101> dislocations are observed above the "knee" for the stoichiometric case. Another possibility is that decomposition of the a<111> dislocation occurs directly into three a<010> dislocations, without an intermediate state involving a<101> dislocations. The former would be favored in the event of higher vacancy diffusivity. Recent data by Collins [10] using the Perturbed Angular Correlation Method indeed suggest that vacancy motion initiates at around 600 K, and that the stoichiometric compound contains a higher density of vacancies. Further studies of alternative paths for a<111> decomposition are necessary to clarify this issue.

Acknowledgments

Support for this project was provided by the Department of Energy under Grant # DE-FG-02-96ER45550 (for MJM, SR and MFS), as well as the National Science Foundation under Grant # 95-10259 (for MSD).

References

1. V. I. Levit, I. A. Bul, J. Hal, and M. J. Kaufman, Scripta Metall. Mater. 34, 1925 (1996).
2. R. D. Noebe and A. Garg, NASA TM 106981 (August 1995).
3. H. L. Fraser, R. E. Smallman, and M. H. Loretto, Philos. Mag. A. 28, 651 (1973).
4. R. D. Field, D. F. Lahrman, and R. Darolia, Acta Metall. Mater. 39, 2951 (1991).
5. C. L. Fu and M. H. Yoo, Acta Metall. Mater. 40, 703 (1992).
6. C. H. Lloyd and M. H. Loretto, Phys. Stat. Sol. 39, 163 (1970).
7. U. Glatzel, K. R. Forbes, and W. D. Nix, Phil. Mag. A 67, 307 (1993).
8. M. J. Mills, R. Srinivasan, and M. S. Daw, Philos. Mag. A. Accepted.
9. M. J. Mills and D. B. Miracle, Acta Metall. Mater. 41, 85 (1993).
10. G. S. Collins, J. Fan, and B. Bai, Structural Intermetallics 1997, eds. M. V. Nathal et al., p. 43, TMS Publications, (1997).